analytical chemistry

Article

pubs.acs.org/ac

NMR Nanoparticle Diffusometry in Hydrogels: Enhancing Sensitivity and Selectivity

Daan W. de Kort,[†,∥] John P. M. van Duynhoven,*[,†,‡,∥] Freek J. M. Hoeben,[§,∥] Henk M. Janssen,[§,∥] and Henk Van As[†,∥]

[†]Laboratory of Biophysics and NMR Centre, Wageningen University, Dreijenlaan 3, 6703 HA Wageningen, The Netherlands

[‡]Unilever R&D, Olivier van Noortlaan 120, 3133 AT Vlaardingen, The Netherlands

[§]SyMO-Chem B.V., Den Dolech 2, 5612 AZ Eindhoven, The Netherlands

[∥]TI-COAST, Science Park 904, 1098 XH Amsterdam, The Netherlands

Supporting Information

ABSTRACT: From the diffusional behavior of nanoparticles in heterogeneous hydrogels, quantitative information about submicron structural features of the polymer matrix can be derived. Pulsed-gradient spin−echo NMR is often the method of choice because it measures diffusion of the whole ensemble of nanoparticles. However, in ^{1}H diffusion-ordered spectroscopy (DOSY), low-intensity nanoparticle signals have to be separated from a highly protonated background. To circumvent this, we prepared ^{19}F labeled, PEGylated, water-soluble dendritic nanoparticles with a ^{19}F loading of ∼7 wt % to enable background free ^{19}F DOSY experiments. ^{19}F nanoparticle diffusometry was benchmarked against ^{1}H diffusion-T_2 correlation spectroscopy (DRCOSY), which has a stronger signal separation potential than the commonly used ^{1}H DOSY experiment. We used bootstrap data resampling to estimate confidence intervals and stabilize 2D-Laplace inversion of DRCOSY data with high noise levels and artifacts, allowing quantitative diffusometry even at low magnetic field strengths (30 MHz). The employed methods offer significant advantages in terms of sensitivity and selectivity.

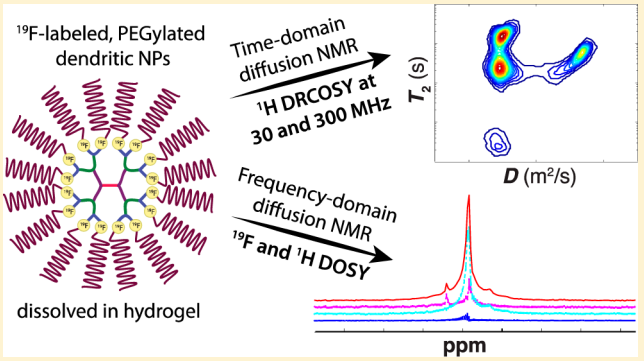

Biopolymer-based hydrogels are widely applied in technological applications, such as barrier and separation materials, controlled release media, and in foods and cosmetics. They derive many of their technologically relevant physical parameters from their submicron structural features. Traditionally, these features have been studied by (electron) microscopic techniques, but these methods are invasive and require careful image analysis in order to quantify network parameters. An increasingly popular method for the noninvasive characterization of heterogeneous hydrogels is through the observation of hindered diffusion of embedded nanoparticles with diameters in the 1−100 nm range. Physical models are available to describe hindered diffusion of nanoparticles in polymer gels[1] and solutions[2] in terms of structural length scales and dynamics. These physical models allow quantitative network descriptors to be derived from experimental nanoparticle diffusion data. Quantitative nanoparticle diffusometry has been convincingly demonstrated in various biopolymer model systems, including alginate,[3] kappa-carrageenan,[4] casein,[5,6] gelatin,[7] whey,[8] and collagen[9] gels.

Optical methods to measure nanoparticle self-diffusion in complex materials, including fluorescence recovery after photobleaching[10,11] (FRAP) and fluorescence correlation spectroscopy[12] (FCS), require fluorescent labeling of particles and optical transparency of the material. Particularly in heterogeneous biopolymer gels, optical transparency issues limit the use of these methods.

For diffusion measurements by NMR, we need nanoparticles with NMR-observable nuclei in molecular segments with liquidlike reorientation dynamics. Optical transparency of the material is, however, not required. For this reason, NMR is as a robust method for nanoparticle diffusometry in biopolymer gels.

Dendrimers are ideal diffusional probes because they are essentially monodisperse due to controlled, stepwise size increments during synthesis.[13] Nanoparticles are observed from their ^{1}H signals, but since they are typically dosed at low levels (∼0.1 wt %) in order not to perturb submicron structure, ^{1}H diffusometry suffers from low selectivity for particles against a highly protonated background of water and polymer matrix. Although water and matrix signals can, for a large part, be suppressed through spectral editing,[14] any

Received: June 15, 2014
Accepted: August 20, 2014
Published: August 20, 2014

   dx.doi.org/10.1021/ac502211q | Anal. Chem. 2014, 86, 9229−9235

remaining background signal can cause difficulties in the interpretation of nanoparticle diffusometry experiments.

One route to overcome the selectivity issues of ^{1}H NMR nanoparticle diffusometry is to label them with an NMR observable isotope that is otherwise not present in the hydrogel matrix. Due to its high gyromagnetic ratio, labeling nanoparticles with ^{19}F is attractive and will allow for sensitive and background-free detection.

A second route to achieve optimal separation of nanoparticle and background signals is to use diffusion-T_2 relaxation correlation spectroscopy (DRCOSY) instead of the more commonly used diffusion-ordered spectroscopy (DOSY). T_2, the spin−spin relaxation time, is the time constant that describes how fast transverse magnetization decays to zero. The building blocks of these techniques and required data transformations are summarized in Table 1.

Table 1. DOSY and DRCOSY Experiments: Building Blocks[a]

	F_2	F_1 acquisition	transformations/fitting procedures
DOSY	PGSE	FID	F_1: Fourier transform
			F_2: Discrete exponential fit (SplMod[15])
DRCOSY	PGSE	time-domain CPMG	F_2, F_1: 2D Laplace inversion (FLI[19])

[a]Building blocks of diffusion-ordered spectroscopy (DOSY) and diffusion-relaxation correlation spectroscopy (DRCOSY) experiments, and their data transformations, are indicated. The PGSE block is based on the stimulated echo: $90°-G-90°-\tau_z-90°-G$, where diffusion observation time equals the time between gradient pulses G. DOSY is composed of a pulsed-gradient spin−echo (PGSE) type diffusion block in the F_2 domain followed by acquisition of the free induction decay (FID) in F_1. FIDs are Fourier transformed to obtain NMR spectra. Spectra are then fitted with a discrete sum of attenuation exponentials using SplMod.[15] DRCOSY is composed of a PGSE type diffusion experiment followed by time-domain Carr−Purcell−Meiboom−Gill (CPMG, $[180°-\tau_e]_n$, where τ_e equals interecho time) acquisition. Two-dimensional Laplace inversion (2D-ILT) using a fast algorithm[19] yields the diffusion-T_2 correlation map.

In DOSY, free-induction decays (FID) are Fourier-transformed to obtain NMR spectra, and the pulsed gradient spin echo (PGSE) dimension is fitted with attenuation exponentials using appropriate procedures, such as SplMod,[15] CONTIN,[16] or multivariate methods,[17,18] to obtain associated diffusion coefficients. Here, we will be using SplMod because of its ability to handle exponential sampling of the gradient axis and perform a "coupled fit" of all spectral points, resulting in a spectral decomposition.

DRCOSY is a correlation experiment that combines the PGSE and Carr−Purcell−Meiboom−Gill (CPMG) experiments. Acquisition of the NMR signal takes place in the time domain (i.e., all echo intensities are recorded during the CPMG experiment). Time domain acquisition allows the total acquisition time of DRCOSY to equal that of DOSY. 2D Laplace inversion of the data yields a diffusion-T_2 correlation map.

Here, we compare DOSY and DRCOSY ^{19}F and ^{1}H NMR diffusometry of ^{19}F-labeled, PEGylated dendrimer nanoparticles (SyMO-Chem B.V.) in a kappa-carrageenan gel model system. We performed ^{19}F and ^{1}H DOSY at 7 T field strength and ^{1}H DROSY at 7 and 0.7 T field strength (Table 2). ^{19}F DRCOSY at high field was not performed, since it does not offer advantages over ^{19}F DOSY in which only a single chemical shift is present. DOSY is then preferred over DRCOSY because of the stability of FT over Laplace inversion.

Table 2. Diffusometry Experiments in This Work[a]

	high field 7.0 T	low field 0.7 T
DRCOSY	^{1}H	^{1}H
DOSY	^{1}H ^{19}F	n/a

[a]DOSY experiments typically cannot be performed at low field strength because of poor magnet homogeneity in combination with low chemical shift separation of signals. ^{19}F experiments were not performed at low field strength because of low sensitivity due to the relatively small ^{19}F payload per particle and low particle concentrations.

Kappa-carrageenan gels were chosen as the model system because of their submicron structural heterogeneity. Lorén et al. observed bimodal diffusion of nanoparticles in kappa-carrageenan gels, which could be a result of the presence of microdomains in which nanoparticles have truly different diffusion coefficients.[4] We will assess the performance of both DOSY and DRCOSY for resolving bimodality of diffusion.

EXPERIMENTAL SECTION

Design of Labeled Nanoparticles. Poly(propyleneimine) (PPI)-based dendrimers were used as a chassis for constructing ^{19}F labeled nanoparticles (SyMO-Chem B.V.). Three generations (G1, G3, and G5) of PPI dendrimers were functionalized with $C^{19}F_3$ and coated with PEG (Figure 1). PEGylation solubilizes the particles and prevents interactions between the particles and the biopolymer matrix. In order to avoid compromised solubility of the dendrimers, the hydrophobic $C^{19}F_3$ functional groups were introduced at the interface between dendritic core and PEG corona.

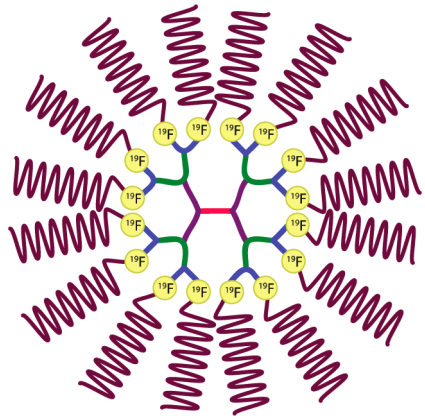

Figure 1. Design of $C^{19}F_3$-functionalized nanoparticles based on polypropylene-imine dendrimer cores of generations G1, G3, and G5 and a polyethylene glycol (PEG) corona, which prevents sticking of particles to the biopolymer network. ^{19}F-labels have been introduced at the interface between the dendritic core and PEG corona.

NMR Relaxometry. ^{19}F-labeled, PEGylated dendritic nanoparticles were characterized by ^{19}F and ^{1}H relaxometry. Experiments were performed on a Bruker Avance II spectrometer, equipped with a Bruker diff25 probe, at 7.0 T

dx.doi.org/10.1021/ac502211q | Anal. Chem. 2014, 86, 9229−9235

(300 MHz for ^{1}H and 282 MHz for ^{19}F), in water at 298 K. The probe was equipped with a 10 mm RF insert that could be tuned to both ^{1}H and ^{19}F. Sample volume was chosen as to not exceed the NMR coil volume. Longitudinal relaxation (T_1) was measured by an inversion−recovery experiment (180°−τ_{ir}−90°). Transverse relaxation (T_2) was measured by a frequency-domain CPMG experiment with an interecho time of 1 ms. In the ^{1}H case, PGSE diffusion editing was used to suppress the water signal.

Preparation of Kappa-Carrageenan Gels. Kappa-carrageenan gels were prepared by dissolution of kappa-carrageenan powder (Sigma-Aldrich), NaCl and KCl salts, and nanoparticles in water, as described by Lorén et al.[4] Kappa-carrageenan weight fraction was varied between 1% and 5% in five steps. In all experiments, nanoparticles were dosed at 0.1 wt %; NaCl concentration was kept at 200 mM and KCl concentration at 20 mM. Molten gels were transferred into NMR tubes, where the filling height was chosen not to exceed the linear part of the magnetic field gradient. Gels were allowed to stabilize for 24 h before measurements were performed.

NMR Diffusometry. PGSE experiments were carried out by stepwise variation of the gradient pulse amplitude, while keeping the diffusion-observation time and gradient pulse width constant. The attenuation of signal intensity as a function of the experimental parameters is described by the Stejskal−Tanner equation $(I/I_0) = e^{-q^2(\Delta - \delta/3)D}$, where (I/I_0) is the signal attenuation, Δ the effective diffusion time (s), D the diffusion coefficient (m^2 s^{-1}) and $q = \gamma\delta g$, where γ is the gyromagnetic ratio of the observed nucleus (rad T^{-1} s^{-1}), g is the magnetic field gradient amplitude (T m^{-1}), and δ is the effective gradient pulse width (s), where $\delta \ll \Delta$ (narrow gradient pulse approximation).[20] Bimodality of diffusion in heterogeneous gels can manifest itself through biexponential attenuation of the NMR signal with increasing gradient strength.[4] This means that a curve of signal intensity versus q can be fitted with a discrete sum of attenuation exponentials $(I/I_0) = \sum_i A_i e^{-q^2(\Delta - \delta/3)D_i}$, where A_i is the amplitude and D_i the diffusion coefficient of component i.

Apparatus. High-field ^{19}F and ^{1}H DOSY and ^{1}H DRCOSY NMR experiments were performed on a Bruker Avance II spectrometer at 7.0 T equipped with a Bruker diff25 gradient probe, as described above. This probe generates a maximum field gradient strength of 9.6 T m^{-1}. Sample temperature was kept at 293 K, regulated indirectly through the gradient-coil cooling system to prevent any temperature gradients across the sample. Low field ^{1}H DRCOSY experiments were performed on a Maran Ultra spectrometer equipped with a 0.7 T permanent magnet (30 MHz for ^{1}H), equipped with a magnetic field gradient coil that generates a maximum gradient strength of 1.2 T m^{-1}. Low field experiments were performed at room temperature.

^{1}H (300 MHz) and ^{19}F (282 MHz) DOSY. DOSY experiments were performed on G1, G3, and G5 dendrimers in water and carrageenan gels. A stimulated echo-based PGSE diffusion experiment was used in combination with unipolar, trapezoid-shaped gradient pulses. In all DOSY experiments, an effective diffusion time Δ of 200 ms was used and an effective gradient pulse width δ of 1.5 ms. The gradient strength was varied in a logarithmic manner between 0.5−4.5 T m^{-1} for ^{1}H and 0.03−4.5 T m^{-1} for ^{19}F in 64 steps. A stimulated-echo-based PGSE experiment requires nonzero initial gradient amplitude. However, the initial gradient was stronger in the ^{1}H case than in the ^{19}F case in order to effectively suppress the intense ^{1}H signal of water, whose diffusion coefficient is over 10 times higher than that of dendrimer nanoparticles. For ^{1}H NMR measurements, the NMR signal was averaged 16 times and for ^{19}F NMR 64 times. Experimental repetition time was set at 3 times T_1 of PEG and ^{19}F labels, respectively.

High-Field ^{1}H (300 MHz) DRCOSY. High-field DRCOSY experiments were performed on G1, G3, and G5 dendrimers in water and carrageenan gels. Experiments were based on a stimulated echo-based PGSE diffusion experiment with unipolar, trapezoid-shaped gradient pulses, followed by time-domain CPMG acquisition. Experimental parameters for the PGSE block were the same as those used in ^{1}H DOSY. For CPMG, an interecho time of 1 ms was used, and 2048 echo intensities were recorded. The NMR signal was averaged 16 times. Experimental repetition time was set at 3 times T_1 of PEG.

Low-Field ^{1}H (30 MHz) DRCOSY. Low-field DRCOSY experiments were performed on G3 dendrimers in water and carrageenan gels. The experimental parameters for the PGSE and CPMG blocks were identical to those used for high-field DRCOSY, except that gradient strength was varied in a logarithmic manner between 0.5−1.2 T m^{-1} in 64 steps. The NMR signal was averaged 256 times. Experimental repetition time was set at 3 times T_1 of PEG.

Data Analysis. We used bootstrap data resampling[21] as a simple but effective tool to estimate confidence intervals in PGSE and CPMG data. Furthermore, we found that bootstrap resampling is an effective method to stabilize 2D Laplace inversion of DRCOSY data subject to high noise levels and artifacts that would otherwise lead to "spurious" peaks in the D-T_2 correlation maps.

Bootstrap resampling was implemented as transformation of subsequent random subselections of data points and summation of the resulting intensity spectra or correlation maps. Bootstrapping is an adequate statistical method because the distribution of statistics (diffusion coefficient, T_2) is not known (deviations from the bimodal model might occur in the case of diffusive exchange), and the sample size is low, particularly in the PGSE dimension ($\sim 10^1$ data points). Previously, random addition of noise has been used as an analogous method to estimate errors in PGSE data.[22] Bootstrap resampling, however, does not manipulate data points and offers the additional benefit of evaluating model robustness, besides evaluating the effects of noise.

Analysis of DOSY Experiments. NMR spectra were obtained through Fourier transformation of FIDs and subsequent phasing using standard procedures. In the PGSE dimension, 1000 bootstrap samples of 64 spectra were prepared. These 1000 bootstrap samples were successively fitted with 1−3 attenuation exponentials through SplMod.[15,23] For analyzing ^{1}H NMR diffusometric data, SplMod was used in the coupled mode in order to achieve spectral decomposition. The nonzero initial gradient amplitude was set to $q = 0$ in order to suppress the water signal in the resulting intensity spectra. This procedure only changes the point at which the attenuation curve intercepts the amplitude axis and does not influence the estimated diffusion coefficients, which follow from the attenuation rate as a function of q. In the ^{19}F case, the single C^{19}F$_3$ resonance was integrated and fitted by SplMod (not in coupled mode because spectral decomposition is not required). Basic bootstrapped confidence limits were obtained by finding

dx.doi.org/10.1021/ac502211q | Anal. Chem. 2014, 86, 9229−9235

Table 3. Physical Properties of PPI Dendrimer Constructs[a]

PPI dendrimer generation			G1	G3	G5
hydrodynamic diameter (nm)			2.76	4.58	6.90
molar mass (kDa)			3.156	13.043	52.592
mass fraction ^{19}F (wt %)			7.2	7.0	6.9
T_1 (ms)	^{1}H, PEG	−3.7 ppm	633 ± 20	538 ± 18	529 ± 23
	^{19}F, −C^{19}F$_3$	−64 ppm	620 ± 12	561 ± 11	412 ± 15
T_2 (ms)	^{1}H, PEG	−3.7 ppm	589 ± 25	505 ± 28	375 ± 30
	^{19}F, −C^{19}F$_3$	−64 ppm	400 ± 10	240 ± 12	129 ± 12

[a]Characterization of functionalized G1, G3, and G5 poly(propyleneimine) (PPI) dendritic nanoparticles. Hydrodynamic diameters were calculated from diffusion coefficients in water at 298 K through the Stokes−Einstein equation. Relaxation parameters were measured at 7.0 T.

the median and one-standard-deviation quantiles of the relevant parameters.[24]

Analysis of DRCOSY Experiments. A zeroth-order phase correction was applied to the CPMG echo train. Subsequently, the data were bootstrapped and analyzed through Fast 2D Laplace Inversion (FLI).[19] As in ^{1}H DOSY, the intense water signal was suppressed by a strong initial gradient. The PGSE axis, which starts at a nonzero value, was again shifted to zero initial gradient amplitude (q = 0), in order to suppress the intense water signal. Before 2D Laplace inversion, 250 bootstrap samples were prepared of both the PGSE and CPMG dimensions and combined into 250 two-dimensional reference matrices. Data points selected through these matrices were subsequently inverted by FLI. For all bootstrap fits, the regularization ("smoothing") parameter was fixed at a low value. Because FLI output is the intensity map back-predicted to (t = 0, q = 0), resulting maps could simply be summed to obtain an averaged map, in which robust elements would survive and spurious peaks would disappear. Unlike in the DOSY case, bootstrapped parameter distributions could not be obtained directly. Instead, we determined the signal width (fwhm) in the bootstrapped intensity map in order to estimate the error.

RESULTS AND DISCUSSION

Characterization of ^{19}F-Labeled Dendrimers. By attaching ^{19}F labels in-between dendritic cores and PEG coronas, we introduced ^{19}F payloads of ∼7 wt % without affecting the water solubility of the dendrimer constructs. In the current design, the ratio between ^{19}F nuclei and PEG ^{1}H nuclei is 1:15. Higher ^{19}F payloads should be attainable with the used PPI architectures via a similar design. ^{19}F NMR spectra of three generations of C^{19}F$_3$-functionalized dendritic nanoparticles showed a single resonance line (−64 ppm). The ^{1}H spectrum showed a prominent signal from the PEG corona (3.7 ppm) and several broad dendritic signals. Relaxation parameters of ^{19}F labels and PEG groups at 7.0 T are presented in Table 3. Longitudinal (T_1) and transverse (T_2) relaxation times of polyethylene glycol (PEG) corona and ^{19}F labels at 7.0 T field strength allow for diffusion-observation times of order 10^1−10^2 ms. Although it can be predicted that the use of spin−echo-based PGSE would result in a higher S/N than the use of a stimulated echo, we chose to use stimulated-echo-based PGSE, because T_2 might shift to lower values when nanoparticles are embedded in dense polymer gels. Hydrodynamic diameters of nanoparticles were estimated from their diffusion coefficients in water at 298 K, as measured by DOSY, through the Stokes−Einstein equation $3\pi\eta d_h D = k_b T$, where η is solvent dynamic viscosity (1.002 mPa s for water at 298 K), d_h the hydrodynamic particle diameter, D the diffusion coefficient, k_b the Boltzmann constant, and T the temperature. Hydrodynamic particle diameters were found to be 2.76, 4.58, and 6.90 nm for G1, G3, and G5 dendrimers, respectively. Nanoparticles dissolved in water and stored at room temperature were stable over periods of months, as confirmed by invariant ^{19}F and ^{1}H NMR spectra and self-diffusion coefficients.

NMR Diffusometry. In heterogeneous systems, multimodal diffusion will be observed only at timescales smaller than required for particles to exchange between different domains. At longer timescales, a single diffusion coefficient will be observed again (central limit theorem). In kappa-carrageenan gels, varying the experimental diffusion-observation time did not change the apparent diffusion behavior. This implies that particle exchange is much slower than typical diffusion-observation times accessible with PGSE NMR. We consequently chose a diffusion observation time of 200 ms, at which the narrow gradient pulse requirement is satisfied.

^{19}F (282 MHz) and ^{1}H (300 MHz) DOSY. Because pulsed-field gradient probeheads require smaller-than-usual sample volumes in view of gradient linearity requirements, it is difficult to obtain high magnetic field homogeneity within the sample ("shimming"). This leads to strong overlap of signals in the NMR spectrum. DOSY, which relies on acquisition of the NMR spectrum, did therefore not strongly separate nanoparticle and background signals adequately in the spectral domain. We fitted up to three attenuation exponentials to both ^{1}H and ^{19}F DOSY spectra, and the resulting diffusion coefficients and bootstrapped error intervals were calculated.

A representative three-component spectral decomposition of the ^{1}H DOSY data is presented in Figure 2. It can be seen that all signals are broad and distorted, due to low magnetic field homogeneity. The first component, which has the largest diffusion coefficient (∼10^{-10} m^2 s^{-1}), corresponds to sucrose

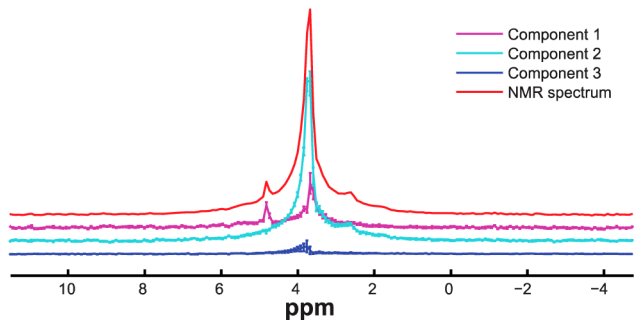

Figure 2. Representative result of ^{1}H DOSY three-component spectral decomposition by SplMod in coupled mode (5 wt % carrageenan containing 0.1 wt % G5 dendrimers). Error bars represent 1 standard deviation.

dx.doi.org/10.1021/ac502211q | Anal. Chem. 2014, 86, 9229−9235

(with a contribution of nonsuppressed water), an impurity in some of the commercially available kappa-carrageenan batches (Section S−3 of the Supporting Information). The sucrose NMR spectrum includes a broad range of chemical shifts in the sugar region. The second component ($D \sim 10^{-11}$ m^2 s^{-1}) corresponds to the PEG corona of the dendrimer particles. The diffusion coefficient of this component decreases as a function of kappa-carrageenan concentration. From this effect, structural properties of the matrix can be calculated through physical models of diffusion in polymer gels.[1] The third component ($D \sim 10^{-13}$ m^2 s^{-1}) can correspond to slow-diffusing particles, (immobile) kappa-carrageenan matrix (Figure S3 of the Supporting Information) or both. The presence of a slow-diffusing particle fraction can either indicate the presence of microdomains with different polymer densities in which particles have different diffusion coefficients or that the polymer matrix acts as a confinement in which particles can become restricted in their diffusion. In ^{1}H DOSY, however, slow-diffusing particles and kappa-carrageenan signal cannot be properly separated due to both their low intensities and low diffusion coefficients. Low diffusion coefficients are difficult to resolve due to limited PFG amplitudes. From ^{1}H DOSY alone, the existence of a slow-diffusing fraction can therefore not be unambiguously established.

In ^{19}F DOSY, water, solutes, and matrix signals are not present. We have compared one- and two-component models for ^{19}F with the three-component model for ^{1}H DOSY. If a slow-diffusing particle fraction is indeed present, we expect to observe two components in ^{19}F DOSY data. In Figure 3, top, it can be seen that for all particles, close overlap of ^{19}F data with the second component of ^{1}H DOSY is found with a one-component fit of ^{19}F data. However, (only) for G5 particles, a two-component fit also gives satisfactory agreement with the ^{1}H data. Furthermore, for G5 particles, fitting a second component leads to a relatively strong decrease of the standard deviation of the fit (Figures S-2c, g, h, i of the Supporting Information). We thus find a slow-diffusing particle fraction only for G5 particles. As was the case for ^{1}H DOSY, the slow-diffusing fraction is ill-resolved due to its low intensity and diffusion coefficient. It can be seen in Figure 3, however, that the ^{1}H DOSY, third component and ^{19}F DOSY, second component for G5 particles are in agreement within the same order of magnitude.

^{1}H DRCOSY at High (300 MHz) and Low (30 MHz) Field Strengths. Since DRCOSY does not rely on separation of signals on the basis of chemical shift, there is no requirement for the magnetic field to be as homogeneous as for the DOSY case. During CPMG, successive spin echoes will refocus dephasing due to static field inhomogeneity. Since there is no need for spectral resolution, DRCOSY can also be used at low field strengths. At first sight, therefore, DRCOSY seems a more appropriate method for nanoparticle diffusometry. A drawback of DRCOSY, however, is the necessity to use 2D Laplace inversion to obtain the diffusion-T_2 relaxation correlation map. Laplace inversion is an ill-conditioned problem in that the signal matrix cannot be inverted robustly under the effects noise and signal artifacts, and a large number of solutions exist that fit the data within the experimental error. A small change in the signal (e.g., due to noise or artifacts) can lead to a large change in the solution. Generally, the output is the simplest (most parsimonious) solution that is consistent with experimental data, generally with smoothness of the distribution as a constraint.[16] Standard regularization methods for 2D Laplace

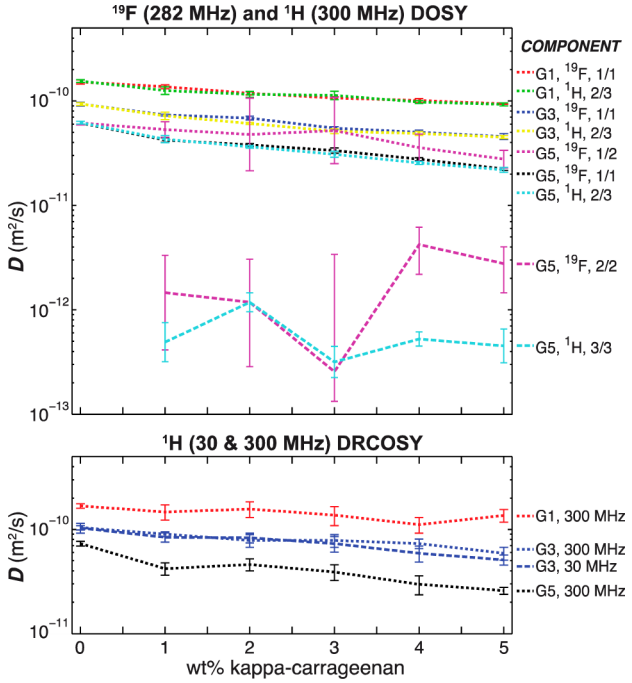

Figure 3. Diffusion of G1, G3, and G5 dendritic nanoparticles in kappa-carrageenan. Diffusion coefficients derived from SplMod fits of ^{19}F DOSY and coupled SplMod fits of ^{1}H DOSY spectra (top). Error bars represent 1 standard deviation. ^{19}F DOSY spectra were fitted with one component for G1 and G3 and G5 and two components for G5. ^{1}H DOSY spectra were fitted with three exponentials. For ^{1}H, only nanoparticle-associated components are shown. Diffusion coefficients derived from ^{1}H DRCOSY at high and low field, fast diffusing fraction only (bottom). For DRCOSY, errors were estimated from correlation peak width in bootstrap-resampled diffusion−T_2 maps.

inversions such as Tikhonov regularization are used to impose this smoothness. This way, noise-free solutions are obtained, but the solution is generally oversmoothed.[25]

Due to the low dosage levels of nanoparticles, noise and artifacts (e.g., small echo modulations due to spectrometer imperfections) become significant. Here, we use very little regularization and alternatively use bootstrap data resampling both as a tool to estimate confidence intervals and to average out the effects of noise and artifacts. We prefer bootstrapping to regularization because we found that regularization does not stabilize our correlation maps as consistently as bootstrapping. The cause of this must lie in the effects of signal artifacts rather than of noise. As opposed to noise, artifacts are not necessarily randomly distributed, which can lead to a consistent peak in the $D-T_2$ correlation maps. Bootstrapping will remove peaks of such artifacts, at least if they cannot be described by an exponential function.

We have illustrated the effects of bootstrap resampling in Figure 4, where we compare diffusion-T_2 correlation maps of raw and bootstrapped data. Bootstrapping leads to a stabilization of diffusion-T_2 correlation maps, as can be seen from the fact that signals in bootstrapped maps persist in all samples (cf. section S−1 of the Supporting Information). When comparing the two maps, it can be seen that bootstrap resampling removes some spurious signals and broadens persistent correlation peaks. The additional broadening introduced by bootstrap data resampling can be interpreted as a measure for the confidence interval of diffusion coefficients and T_2 relaxation times.

dx.doi.org/10.1021/ac502211q | *Anal. Chem.* 2014, 86, 9229−9235

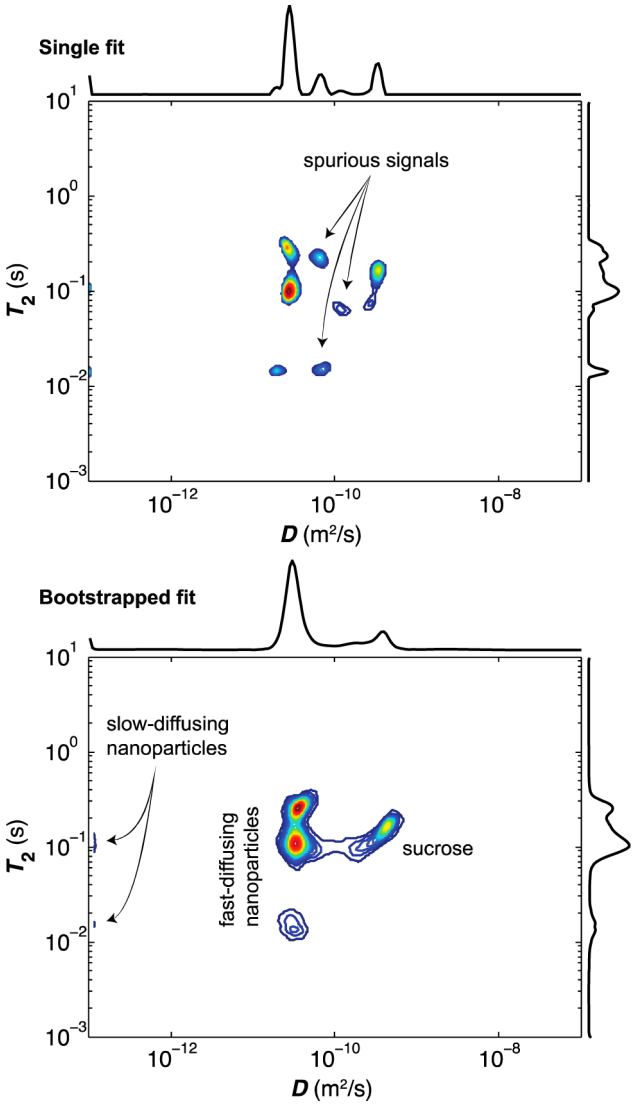

Figure 4. Representative ^{1}H diffusion-T_2 relaxation correlation maps of dendritic nanoparticles in kappa-carrageenan gels (4 wt % kappa-carrageenan, G5 dendrimers). Single fit of raw data is shown (top) and the fit of bootstrap-resampled data (bottom).

In general, nanoparticles give rise to three correlation peaks with a common diffusion coefficient. As determined by a CPMG pulse train with subsequent acquisition of the NMR spectrum, the component with the longest T_2 corresponds to PEG, which is the most mobile part of the particles. Shorter T_2 signals correspond to protons more to the interior of the particles. A signal from sucrose is also visible, as well as two signals that most probably correspond to slow-diffusing particles because their T_2 values correspond to those of fast-diffusing particles. Because this intensity appears at the very edge of the correlation map, it is difficult to quantify this fraction in terms of a diffusion coefficient. The slow-diffusing nanoparticle component is observed only in DRCOSY maps of G5 particles, just as we observed this component only in ^{19}F DOSY experiments of G5 particles. Mean diffusion coefficients for the fast-diffusing particle fraction, derived from high and low field DRCOSY experiments are presented in Figure 3, bottom, where they are compared with the diffusion coefficients derived from ^{19}F and ^{1}H DOSY.

Discussion. In this work, we assessed two routes to overcome selectivity issues in NMR nanoparticle diffusometry. The first route relied on ^{19}F labeling of nanoparticles, leading to background-free diffusion measurements but lower sensitivity than for ^{1}H. The second route deployed ^{1}H DRCOSY, instead of DOSY, to achieve a stronger separation between probe and background signals.

While sensitivity of ^{19}F DOSY is lower than ^{1}H DOSY due to the limited number of ^{19}F labels per particle, it is clear from Figure 3, top, that error intervals for the fast-diffusing particle fractions are comparable. With the available sensitivity and PFG power, it is not possible to separate the ^{1}H signal from slow-diffusing particles from the ^{1}H signal from the immobile kappa-carrageenan matrix. Although sensitivity of ^{19}F DOSY is lower due to the limited number of ^{19}F labels per particle, background-free observation of the particles demonstrates the existence of a slow-diffusing particle fraction for G5 particles only.[17] In terms of matrix properties, this indicates that the lower limit of the matrix mesh size is on the order of 5−7 nm, between the diameters of G3 and G5 particles.

In Figure 3, bottom, it can be seen that the experimental error of DRCOSY for the fast-diffusing particle fraction is higher than the error in a three-component fit of ^{1}H or one-component fit of ^{19}F DOSY. However, like ^{19}F DOSY, DRCOSY will offer a better separation of probe and background signals in more complex matrices because signal separation on the basis of T_2 gives a less complex pattern than on the basis of chemical shift. Although this intensity appears at the edge of the correlation map and therefore is difficult to quantify, it does not appear in D-T_2 maps of G1 and G3 particles. This indicates that DRCOSY is able to establish the existence of a slow-diffusing particle fraction where ^{1}H DOSY is not. T_2 offers a much broader separation window than the ∼15 ppm of chemical shift commonly observed in ^{1}H NMR. In fact, in the current setup, the NMR spectrum does not offer any significant potential for separation of signals but rather helps to identify the chemical nature of a component. The advantage of ^{1}H DOSY over DRCOSY in terms of sensitivity thus only exists by the virtue of reliable spectral decomposition, which can only be achieved when fitting a small number of discrete components.

^{19}F DOSY and ^{1}H DRCOSY offer clear advantages over ^{1}H DOSY in terms of sensitivity and resolution. These advantages will become more pronounced in compositionally more complex matrices. At the same time, ^{1}H DOSY is complementary to DRCOSY in that it can give information about the chemical nature of the different components, whereas ^{1}H DRCOSY offers a stronger separation power.

Sensitivity is the only limiting factor for nanoparticle diffusometry at low field strengths. With the current ^{19}F payload, sensitivity at low field strength (28 MHz) is too low at a dosage level of 0.1 wt %. For ^{1}H, it can be seen in the bottom of Figure 3 that the error estimates for high- and low-field DRCOSY are comparable. Although magnetic field strength differed with a factor of 10 (S/N ∼30 times lower), the comparable sensitivity can be accounted for by 16 times more signal averaging, the use of a more sensitive RF coil (solenoid instead of birdcage), and by a longer T_2 for PEG at low field (Figure S-1d of the Supporting Information). We have shown the feasibility of DRCOSY nanoparticle diffusometry on (benchtop) low-field spectrometers.

dx.doi.org/10.1021/ac502211q | Anal. Chem. 2014, 86, 9229−9235

CONCLUSIONS

^{19}F-labeled dendrimer constructs allow for background-free nanoparticle diffusometry studies. However, the ^{19}F payload of the current construct (∼7 wt %) requires a high-field NMR instrument to be used for adequate sensitivity. The employed nanoparticle design does allow for higher ^{19}F-payloads without compromising solubility. ^{1}H NMR diffusometry based on observation of the PEG signal offers higher overall sensitivity, but probe and background signals cannot always be adequately separated. In spite of lower overall sensitivity, ^{19}F DOSY offers superior selectivity and sensitivity for bimodal particle diffusion. As another alternative to ^{1}H DOSY, we demonstrated that ^{1}H DRCOSY has a larger separation power than ^{1}H DOSY at equal overall sensitivity and that bootstrapping is an effective method to stabilize resulting diffusion-T_2 maps toward the effects of noise and artifacts. Bimodal nanoparticle diffusion could be established from both ^{19}F DOSY and ^{1}H DRCOSY. The latter method can be performed using widely available low-field NMR instrumentation.

ASSOCIATED CONTENT

Supporting Information

(S−1) Overview of high- and low-field DRCOSY maps, raw, and bootstrap resampled data fits. (Figure S−1a) Generation 1 dendrimers, 300 MHz. (Figure S−1b) Generation 3 dendrimers, 300 MHz. (Figure S−1c) Generation 5 dendrimers, 300 MHz. (Figure S−1d) Generation 3 dendrimers, 30 MHz. (S−2) Comparison of ^{1}H and ^{19}F DOSY spectral decompositions and their standard deviations. (Figure S−2a) ^{1}H DOSY, three-component fit. (Figure S−2b) ^{19}F DOSY, one-component fit. (Figure S−2c) ^{19}F DOSY, two-component fit. (Figure S−2d) ^{1}H DOSY, G1 dendrimers, residuals. (Figure S−2e) ^{1}H DOSY, G3 dendrimers, residuals. (Figure S−2f) ^{1}H DOSY, G5 dendrimers, residuals. (Figure S−2g) ^{19}F DOSY, G1 dendrimers, residuals. (Figure S−2h) ^{19}F DOSY, G3 dendrimers, residuals. (Figure S−2i) ^{19}F DOSY, G5 dendrimers, residuals. (S−3) NMR spectrum of kappa-carrageenan gel in D_2O; presence of sucrose. Background signal of kappa-carrageenan matrix at high PFG amplitude. (Figure S−3a) NMR spectrum of 3 wt % carrageenan gel at 500 MHz, relative to HDO (4.79 ppm). (Figure S−3b) Same sample, at 300 MHz, as a function of increasing PFG intensity. This material is available free of charge via the Internet at http://pubs.acs.org.

AUTHOR INFORMATION

Corresponding Author

*E-mail: john.vanduynhoven@wur.nl.

Notes

The authors declare no competing financial interest.

ACKNOWLEDGMENTS

We acknowledge Gert-Jan Goudappel, Ewoud van Velzen (Unilever R&D Vlaardingen, NL), and Frank Vergeldt and Alena Průšová (Wageningen University, NL) for technical support and discussions. We thank Yi-Qiao Song (Schlumberger-Doll Research, MA) for providing the FLI algorithm. This research received funding from the Netherlands Organization for Scientific Research (NWO) in the framework of the Technology Area COAST.

REFERENCES

(1) Masaro, L.; Zhu, X. *Prog. Polym. Sci.* **1999**, *24*, 731−775.
(2) Cai, L.-H.; Panyukov, S.; Rubinstein, M. *Macromolecules* **2011**, *44*, 7853−7863.
(3) Bernin, D.; Goudappel, G.-J.; van Ruijven, M.; Altskär, A.; Ström, A.; Rudemo, M.; Hermansson, A.-M.; Nydén, M. *Soft Matter* **2011**, *7*, 5711−5716.
(4) Lorén, N.; Shtykova, L.; Kidman, S.; Jarvoll, P.; Nydén, M.; Hermansson, A.-M. *Biomacromolecules* **2009**, *10*, 275−284.
(5) Salami, S.; Rondeau-Mouro, C.; van Duynhoven, J.; Mariette, F. *J. Agric. Food Chem.* **2013**, *61*, 5870−5879.
(6) Salami, S.; Rondeau-Mouro, C.; van Duynhoven, J.; Mariette, F. *Food Hydrocolloids* **2013**, *31*, 248−255.
(7) Hagman, J.; Lorén, N.; Hermansson, A.-M. *Biomacromolecules* **2010**, *11*, 3359−3366.
(8) Colsenet, R.; Söderman, O.; Mariette, F. *Macromolecules* **2006**, *39*, 1053−1059.
(9) Stylianopoulos, T.; Diop-Frimpong, B.; Munn, L. L.; Jain, R. K. *Biophys. J.* **2010**, *99*, 3119−3128.
(10) Axelrod, D.; Koppel, D. E.; Schlessinger, J.; Elson, E.; Webb, W. W. *Biophys. J.* **1976**, *16*, 1055−1069.
(11) Braeckmans, K.; Peeters, L.; Sanders, N. N.; De Smedt, S. C.; DeMeester, J. *Biophys. J.* **2003**, *85*, 2240−2252.
(12) Rathgeber, S.; Beauvisage, H.-J.; Chevreau, H.; Willenbacher, N.; Oelschlaeger, C. *Langmuir* **2009**, *25*, 6368−6376.
(13) Cheng, Y.; Prud'homme, R. K.; Thomas, J. L. *Macromolecules* **2002**, *35*, 8111−8121.
(14) Liu, M.; Nicholson, J. K.; Lindon, J. C. *Anal. Chem.* **1996**, *68*, 3370−3376.
(15) van Resandt, R. W. W.; Vogel, R. H.; Provencher, S. W. *Rev. Sci. Instrum.* **1982**, *53*, 1392.
(16) Provencher, S. W. *Comput. Phys. Commun.* **1982**, *27*, 229−242.
(17) Huo, R.; Wehrens, R.; van Duynhoven, J.; Buydens, L. M. C. *Anal. Chim. Acta* **2003**, *490*, 231−251.
(18) Nilsson, M.; Morris, G. A. *Magn. Reson. Chem.* **2007**, *45*, 656−660.
(19) Song, Y. Q.; Venkataramanan, L.; Hürlimann, M. D.; Flaum, M.; Frulla, P.; Straley, C. *J. Magn. Reson.* **2002**, *154*, 261−268.
(20) Stejskal, E. O.; Tanner, J. E. *J. Chem. Phys.* **1965**, *42*, 288−292.
(21) Efron, B. *Annals of Statistics* **1979**, *7*, 1−26.
(22) Alper, J. S.; Gelb, R. I. *J. Phys. Chem.* **1990**, *94*, 4747−4751.
(23) Vogel, R. H. *SplMod Users Manual*, version 3; EMBL: Heidelberg, Germany, 1988.
(24) Davison, A. C.; Hinkley, D. V. *Bootstrap Methods and their Application*; Cambridge Series in Statistical and Probablistic Mathematics; Cambridge University Press: Cambridge, U.K., 1997; pp 1−596.
(25) Berman, P.; Levi, O.; Parmet, Y.; Saunders, M.; Wiesman, Z. *Concepts Magn. Reson.* **2013**, *42*, 72−88.